nature communications

Article

https://doi.org/10.1038/s41467-026-70413-3

Predator-driven microbial feedback loops promote plant health

Received: 27 October 2025

Accepted: 26 February 2026

Published online: 14 March 2026

Check for updates

Gen Li[1,2,7], Ting Liu[1,2,3,7] ✉, Huiyu Chuai[1], Huiping Ma[1], Zihan Yang[1], Yangchu Xu[1,2], Huixin Li[1,2,3], Qirong Shen[1,2], Feng Hu[1,2,3], Stefan Geisen[4], Alexandre Jousset[1,5], Zhong Wei[1,2] ✉ & Shane Hogle[6]

Top-down trophic interactions are major drivers of microbiome dynamics, yet their outcomes are difficult to predict and their consequences for pathogen control remain unclear. We combine synthetic bacterial communities of varying complexity with field studies and microcosm assays to test whether microbivorous nematodes reorganize microbiomes to suppress soilborne disease. Field studies show stronger nematode-microbe associations around healthy plants, and microcosm assays confirm that nematode presence produces stable suppression, whereas microbe-only communities collapse under pathogen invasion. Nematode predation depletes non-preferred bacterial taxa and enriches metabolically versatile taxa within Proteobacteria, increasing community-level antagonistic potential and promoting complementary resource-use interactions linked to pathogen inhibition, yielding suppression beyond individual or pairwise effects. A minimal four-component feedback loop linking a nematode predator, plant pathogens, and two plant-associated bacteria with complementary functions accounts for the emergent outcome. Together, these results reveal an animal-mediated pathway of microbiome assembly that enhances resistance to pathogen invasion and provide a trophically informed framework for designing stable, disease-suppressive microbiomes in agriculture.

Soil food webs play a critical role in pathogen suppression through complex trophic interactions[1–5]. While microbe-microbe interactions have recently received increasing attention[6–8], the ecological roles of faunal-microbial interactions in soils remain poorly resolved due to conceptual and methodological challenges[9]. For example, faunal predation on microbes is embedded in microbial communities shaped by mutualism, competition, and antagonism, making it difficult to disentangle direct trophic effects from broader community interactions. As a result, microbial trophic networks remain difficult to predict and quantify, which precludes us from fully leverage the soil microbiome for agricultural purposes.

Here, we investigate how nematodes, one of the dominant consumers of soil bacteria and fungi[10–13], shape root-associated microbiomes to suppress plant pathogens. We focus on *Ralstonia solanacearum*, a globally distributed soilborne pathogen that causes bacterial wilt in over 200 plant species[14]. Using a regional survey and controlled experiments with defined synthetic bacterial communities (SynComs) and representative nematode species, we first assess how nematode predation generally influences the composition and function of root-associated microbiomes. Recent work shows that protist predation reshapes bacterial communities to suppress plant disease[15], but the microbial functions or traits underlying this effect remain

[1]College of Resources and Environmental Sciences, Nanjing Agricultural University, Nanjing, China. [2]Jiangsu Collaborative Innovation Center for Solid Organic Waste Resource Utilization, Nanjing, China. [3]Asia Hub on Agriculture, Sanya Institute of Nanjing Agricultural University, Sanya, China. [4]Laboratory of Nematology, Wageningen University, Wageningen, The Netherlands. [5]Genedance GmbH, Basel, Switzerland. [6]Department of Biology, University of Turku, Turku, Finland. [7]These authors contributed equally: Gen Li, Ting Liu. ✉e-mail: ting.liu@njau.edu.cn; weizhong@njau.edu.cn

unclear. Since predation is known to promote microbial investment in traits such as antibiotic production and competitive resource uptake[16], we hypothesized that nematode predation activates similar microbiome functions that enhance the community's resistance to the pathogen *R. solanacearum*.

We next explore how nematodes interact with specific microbial taxa that mediate pathogen suppression. In soils, nematodes interact with microbial communities through selective predation, which is shaped by microbial traits such as palatability, defense, and metabolic capacity[17]. Our previous work shows that *R. solanacearum* is toxic to nematodes and is actively avoided by them[18], whereas many Proteobacteria are preferentially consumed by nematodes[17,19]. In contrast, Firmicutes and Actinobacteria, often protected by thick cell walls or chemical defenses, are generally not preferred[17,19,20]. This preferential feeding on fast-growing Proteobacteria can stimulate their metabolic activity and initiate positive feedback that reinforce their dominance within the community[12,13,21,22]. We therefore hypothesize that nematode predation promotes the dominance of certain Proteobacteria, which in turn enhances microbial network cohesion and stabilizes microbiome structure under pathogen stress.

To test these hypotheses, we construct a controlled micro-food web system consisting of nematodes, a defined synthetic rhizosphere microbiome, *R. solanacearum*, and tomato plants. The constructed SynCom comprises 122 genome-sequenced bacterial strains spanning dominant cultivable taxa in the tomato rhizosphere, including Proteobacteria, Bacteroidetes, Firmicutes, and Actinobacteria[17]. These groups include key lineages known to promote or inhibit nematode growth and to participate in microbial cooperation or competition[17,23]. Whole-genome sequencing of all strains enables functional metatranscriptomic analysis and precise tracking of bacteria-nematode interactions. This experimental system enables us to investigate how faunal predation influences microbiome structure and function and how these changes suppress plant pathogens.

Results

Nematode presence reduces plant pathogen invasion in the greenhouse

We surveyed 124 agricultural field sites to gain an overview of how the diversity of soil nematodes and bacteria covaries under healthy and diseased plant conditions (Fig. 1a). We sampled rhizosphere soils from healthy plants ($n = 63$) and from diseased plants infected with *R. solanacearum* ($n = 61$) and constructed co-occurrence networks from the relative abundance of bacterial ASVs and nematode species to infer cross-trophic species interactions. Comparison of network topologies

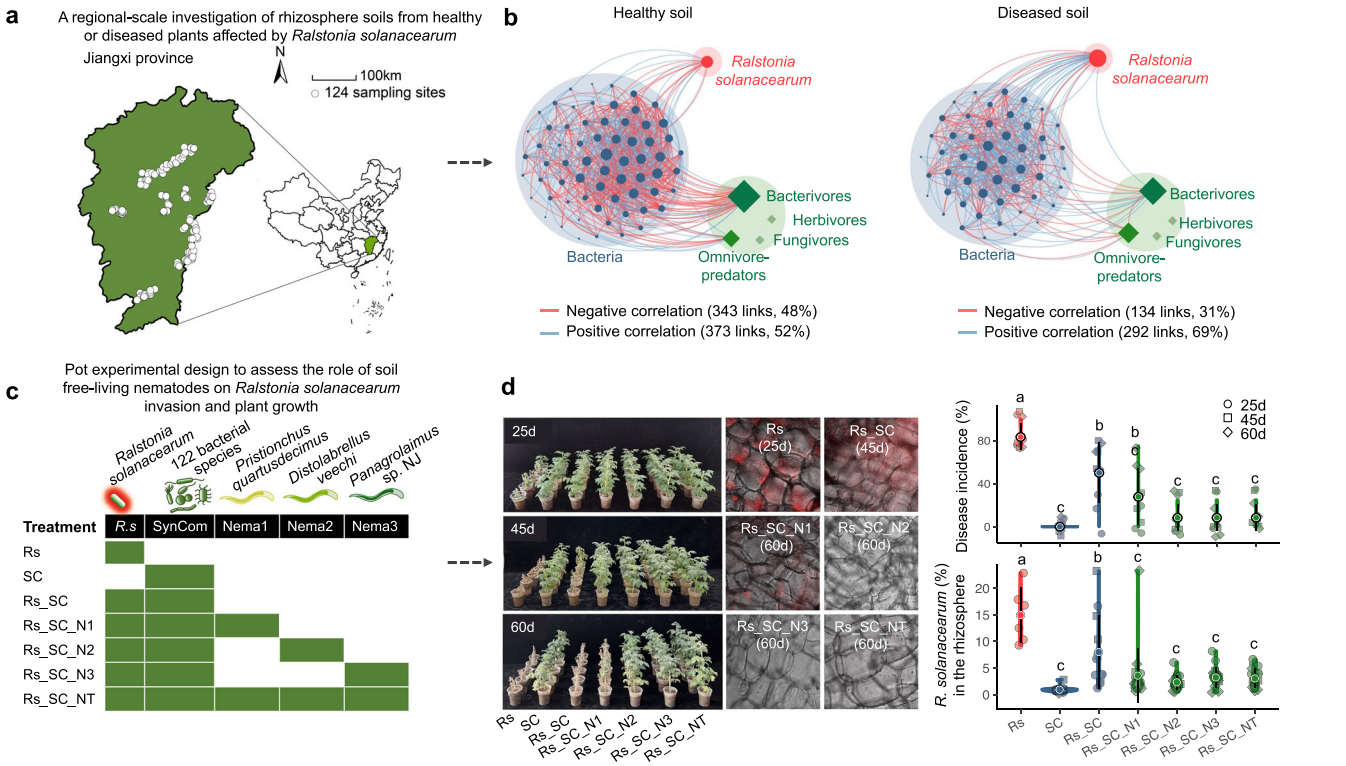

Fig. 1 | Nematode consumers are crucial for plant pathogen suppression. **a** Locations of the 124 rhizosphere soil samples from healthy and *Ralstonia solanacearum* infected plants. **b** Healthy soil is associated with stronger interactions between *R. solanacearum*, bacteria, and nematode communities compared to diseased soil. Co-occurrence networks ($P < 0.05$, $r > 0.3$, sparCC) show the interactions among *R. solanacearum*, bacteria, and nematodes in healthy soil ($n = 63$ biologically independent soil samples) and diseased soil ($n = 61$ biologically independent soil samples). Each bacterial node represents an ASV assigned at the genus level, and each nematode node represents an ASV assigned at the functional group level. Node size is proportional to the number of significant associations. **c** A pot experiment was designed to assess the role of free-living nematodes in *R. solanacearum* suppression. Rs: inoculation of *R. solanacearum*. SC: inoculation of a synthetic community (SynCom) consisting of 122 bacterial strains isolated and constructed from the field investigation. Rs_SC: inoculation of *R. solanacearum* and SynCom. Rs_SC_N1, Rs_SC_N2, Rs_SC_N3, Rs_SC_NT represent inoculation of *R. solanacearum* and SynCom together with the nematode predators *Pristionchus quartusdecimus*, *Distolabrellus veechi*, *Panagrolaimus* sp. NJ, and a combination of the three nematode species, respectively. **d** Nematode inoculation supports better tomato growth and pathogen suppression. Plant growth images and red fluorescent-labeled *R. solanacearum* stem images were captured across treatments at 25, 45 and 60 days. Disease appeared at 25 days for Rs, 45 days for RS_SC, and 60 days for Rs_SC_N1. No disease was observed in the other three nematode treatments (Rs_SC_N2, Rs_SC_N3, Rs_SC_NT) by day 60, so images for these treatments were captured at the same time as for Rs_SC_N1. Disease incidence and *R. solanacearum* densities in the rhizosphere were collected at three sampling times ($n = 6$ biological replicates per sampling time). Data are presented as mean ± SD, with individual data points showing the distribution. Different lowercase letters indicate significant differences among treatments ($P < 0.05$, Kruskal-Wallis chi-squared test with Dunn's post-hoc test).

revealed a higher proportion of negative interactions within bacterial-faunal networks in healthy soils (343 links, 48%) than in diseased soils (134 links, 31%) (Fig. 1b, Supplementary Fig. 1). These were primarily driven by bacterivores, followed by omnivore-predators, but not by fungivores or herbivores (Fig. 1b).

To validate the cross-trophic species correlations observed in the field, we next conducted a tomato greenhouse experiment using a 122-member bacterial SynCom with four trophic treatments including two different bacterivorous nematodes, an omnivorous nematode consuming microbes and other nematodes, and a mixture of bacterivores and the omnivore (Fig. 1c). Tomato plants inoculated with SynCom and *R. solanacearum* were diseased by day 45, while those co-inoculated with nematodes remained healthy up to day 60, except for one treatment with low nematode abundance (Fig. 1d). Fluorescent imaging of stem sections confirmed weak or no *R. solanacearum* colonization in nematode-treated plants (Fig. 1d). Nematode addition reduced rhizosphere pathogen abundance by 63% (Kruskal-Wallis chi-squared = 48.2, df = 6, P = 1e-8), and wilt incidence by 74% compared to the *R. solanacearum*-only control (Kruskal-Wallis chi-squared = 40.3, df = 6, P = 4e-7) (Fig. 1d). Specifically, the two bacterivorous nematodes and the mixed bacterivore-omnivore nematode community showed the strongest pathogen suppression and lowest disease incidence, while the omnivorous nematode was less effective in disease suppression (Fig. 1d). These results confirm that nematodes contribute to pathogen suppression in controlled environments.

Nematode predation reshapes bacterial communities, promoting species evenness

To explore how nematodes affect SynCom dynamics, we conducted a 24-day petri dish experiment with four sequential transfers (on days 6, 12, 18, and 24), comparing SynCom alone versus SynCom with three nematode species (Fig. 2a). Nematode inoculation initially reduced bacterial biomass, but both populations later stabilized (Supplementary Fig. 2). Nematode presence significantly changed bacterial community composition (Bray-Curtis distance, $F_{3,92}$ = 5.4, R^2 = 0.15, p < 0.001, Fig. 2b). Although species richness declined across all treatments (Supplementary Fig. 3a), nematodes increased community evenness (Fig. 2c).

Selective grazing by nematodes enriched Proteobacteria in their gut microbiota, promoting their dominance in the surrounding environment, especially at days 12 and 18 (Kruskal-Wallis chi-squared = 17.6-19.8, df = 3, P < 0.001, Supplementary Fig. 4). Nematode predation reshaped the bacterial community by enriching seven species, including four abundant taxa (> 1% average relative abundance), all of which belonged to the phylum Proteobacteria (Fig. 2d, Supplementary Fig. 3b, Supplementary Table 1). Specifically, nematodes reduced the most dominant species *Paraburkholderia oxyphila* (PAR1, Betaproteobacteria) by 38% (Kruskal-Wallis chi-squared = 13.3, df = 3, P = 0.004), while boosting the less common species *Raoultella ornithinolytica* (RAO1, Gammaproteobacteria) and *Klebsiella michiganensis* (KLE1, Gammaproteobacteria) by 390−420% (Kruskal-Wallis chi-squared = 25.5, df = 3, P = 1e-5, Fig. 2e–g, Supplementary Fig. 3c). These results suggest that top-down trophic control from nematodes promotes a more even microbiome by suppressing dominant species and enriching less common taxa.

Functional changes underlying nematode-driven suppression of plant pathogens

To test whether nematode predation enhances microbiome functions related to pathogen resistance, we assessed two key indicators at the final sampling time (day 24): suppression of *R. solanacearum* and carbon substrate utilization as a proxy for resource competition (Fig. 3a). Pathogen abundance was reduced by 82% compared to the SynCom control (Kruskal-Wallis chi-squared = 14.2, df = 3, P = 0.003, Fig. 3b). Microbial communities also showed a 142% increase in carbon utilization ability and substrate diversity relative to the SynCom control (Kruskal-Wallis chi-squared = 27.3, df = 3, P = 5e-6, Fig. 3c), including broader use of carbohydrates, carboxylic acids, amines, and polymers (Supplementary Fig. 5). These findings indicate that nematodes enhance microbial functional capacity.

To determine whether these functional shifts were reflected at the molecular level, we next conducted metatranscriptomic profiling of the bacterial community at the final sampling time (day 24, Fig. 3a). Nematode predation significantly altered the SynCom's transcriptional profiles at the community level, compared to the SynCom control (Bray-Curtis distance, $F_{3,8}$ = 17.6, R^2 = 0.87, P < 0.001, Fig. 3d, Supplementary Fig. 6a). A total of 19,061 genes showed consistent changes across three nematode treatments, with 60% (11,487 genes) exhibiting increased activity, primarily contributed by KLE1 and RAO1, while most genes with reduced activity were associated with PAR1 (Fig. 3e, f, Supplementary Fig. 6b). Over 80% of the genes with increased activity were involved in metabolic functions, including the biosynthesis of secondary metabolites, antibiotics, amino acids, as well as carbon metabolism (Fig. 3f-g, Supplementary Fig. 7). These molecular signatures, together with enhanced pathogen suppression and carbon utilization capacity, point to a key role of nematode-driven bacterial metabolism in plant pathogen suppression.

Predation triggers positive feedback loops that enhance plant health

The high expression of antibiotic biosynthesis and carbon metabolism genes in KLE1 and RAO1 led us to investigate whether predator-induced interactions between these taxa contribute to pathogen suppression. We conducted fully factorial laboratory microcosms with KLE1, RAO1, and nematodes in the presence of *R. solanacearum*. Nematodes alone did not reduce pathogen abundance (ANOVA: $F_{1,8}$ = 1.48, P = 0.26, Fig. 4a), likely due to impaired growth under pathogen stress (ANOVA: $F_{1,28}$ = 24.8, P < 0.001, Fig. 4b). However, KLE1 and RAO1 individually suppressed pathogens by 70% and 32%, respectively (ANOVA: $F_{1,8}$ = 95-281, P < 0.001, Fig. 4a, Supplementary Fig. 8a). Their co-culture suppressed the pathogen by 79% (Wilcoxon rank-sum test, W = 25, P = 0.008, Fig. 4a), exceeding either monoculture, indicating functional complementarity. This synergy was likely driven by metabolic cross-feeding, as KLE1 grew better in RAO1-conditioned medium than in fresh medium (ANOVA: $F_{1,8}$ = 9.0, P = 0.02, Fig. 4c, d, Supplementary Fig. 8b).

Although nematodes alone did not suppress pathogen density, they strongly modulated the suppressive effects of KLE1 and RAO1. KLE1, the preferred prey, supported higher nematode growth (ANOVA: $F_{1,10}$ = 49.1, P < 0.001, Fig. 4b–e, Supplementary Fig. 8c), although its combination with nematodes did not enhance suppression beyond KLE1 alone (Fig. 4a). In contrast, RAO1, a suboptimal food source (Fig. 4b, c, Supplementary Fig. 8c), showed stronger pathogen suppression when combined with nematodes than when alone (ANOVA: $F_{1,8}$ = 15.2, P = 0.004, Fig. 4a). The RAO1-KLE1-nematode combination suppressed the pathogen more strongly than the RAO1-KLE1 pair (86% vs 79%, ANOVA: $F_{1,8}$ = 8.8, P = 0.02, Fig. 4a). These results reveal a positive feedback loop across trophic levels (Fig. 4f): RAO1 facilitates KLE1 growth, amplifying KLE1-*R. solanacearum* antagonism and providing optimal food for the nematode. Meanwhile, RAO1-nematode interactions enhance RAO1's suppressive effect on the pathogen. Together, the tripartite combination of KLE1, RAO1, and nematode predators achieves stronger suppression than any species or species pair alone.

Importantly, the positive feedback loop observed in petri dishes was validated in greenhouse experiments, where it enhanced both microbial function and plant performance (Fig. 5a). The plant disease index and pathogen density were lowest when all three species were present (Fig. 5b, c). Meanwhile, plant growth (ANOVA: $F_{6,58}$ = 8.5-24.8, Fig. 5d), soil dissolved organic carbon (DOC) (ANOVA: $F_{6,58}$ = 16.1,

https://doi.org/10.1038/s41467-026-70413-3

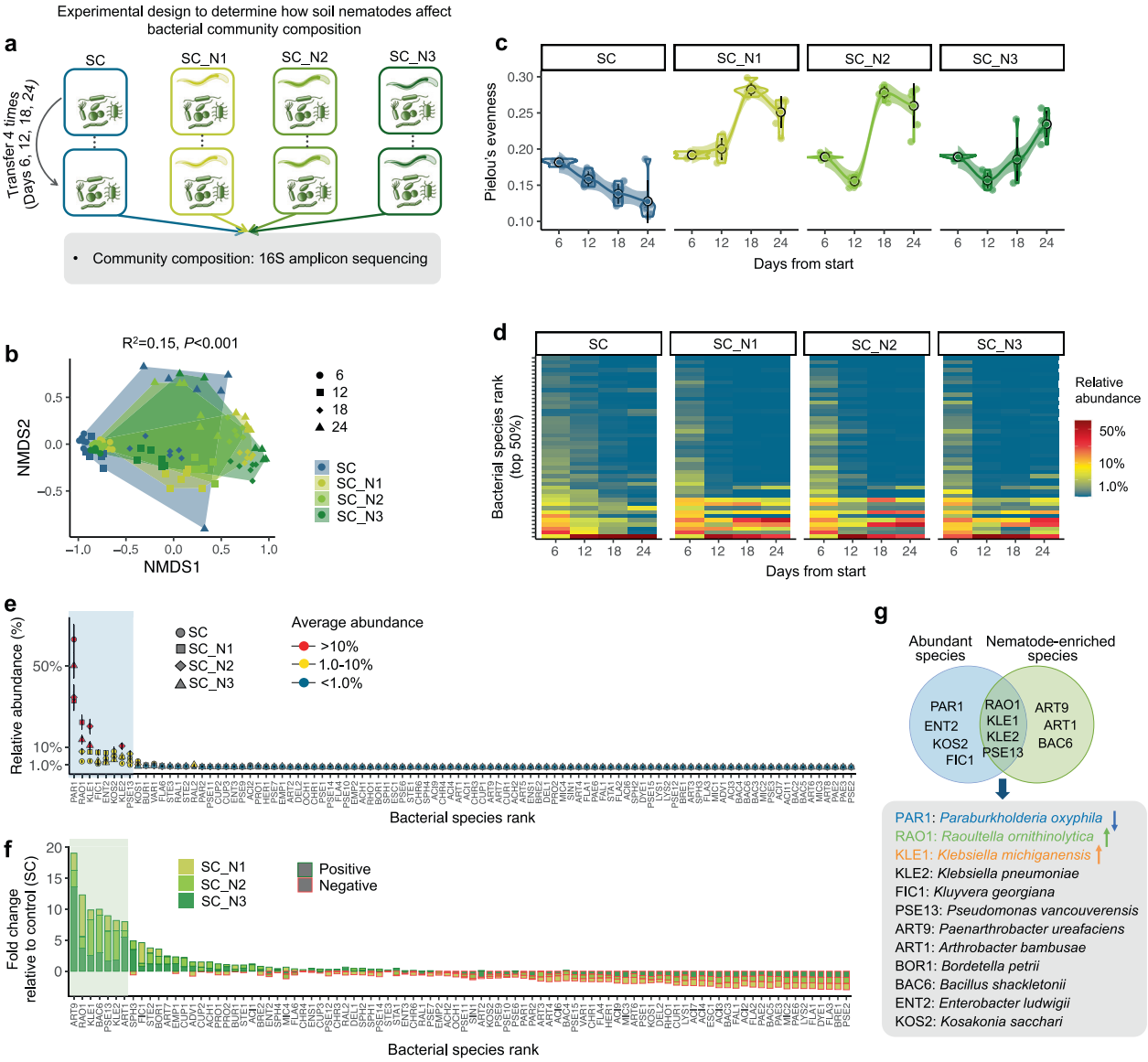

Fig. 2 | Nematode predation alters bacterial community composition. **a** Experimental design assessing the impact of nematodes on bacterial community composition in culture plates mimicking soil conditions. Communities were transferred to new soil conditions due to limited resources on culture plates. Samples of bacterial communities were collected at each transfer time point: 6, 12, 18, and 24 days. SC: synthetic community of 122 bacterial strains (SynCom). SC_N1, SC_N2, and SC_N3: SynCom with nematodes *Caenorhabditis elegans*, *Distolabrellus veechi*, and *Panagrolaimus* sp. NJ, respectively. **b**, Bacterial community composition is reshaped by nematodes during the experiment ($P < 0.001$, PERMANOVA by adonis; $n = 6$ biological replicates per sampling time). **c** Pielou's evenness of the bacterial community is enhanced by nematodes ($n = 6$ biological replicates per sampling time). **d** The distribution of dominant species changes over time under the influence of nematodes. The Y-axis ranks the top 50% bacterial species based on average abundance across six replicates ($n = 6$ biological replicates per sampling time). Data are presented as mean ± SD, with individual data points showing the distribution. **e**–**g** Nematodes reduce the abundance of dominant bacterial species while enriching subdominant ones. The X-axis shows species ranked by relative abundance (**e**), highlighting bacterial species whose abundance increased or decreased in the presence of nematodes compared to the control (SC) (**f**, $n = 24$ biological replicates across four sampling times). **g** summarizes the top species (over 75% in total), highlighting the species that decreased in abundance (PAR1: *Paraburkholderia oxyphila*) and those enriched by nematodes (RAO1: *Raoultella ornithinolytica*, KLE1: *Klebsiella michiganensis*).

$P < 0.001$, Fig. 5e), and bacterial and nematode abundance (ANOVA: $F_{2,27} = 4.0$, $P = 0.03$, Fig. 5f, Supplementary Fig. 9) were highest. Consistent with our in vitro conceptual framework (Fig. 4f), a structural equation model fitted to these data suggests that nematodes enhance plant growth through a trophic cascade, where predation increases bacterial abundance, which in turn suppresses pathogen density and alleviates disease burden on plants (Fig. 5g). Nematodes also increased DOC concentration, which correlated positively with plant growth. Overall, these findings illustrate how greater interaction diversity in soil microbial trophic networks enhances plant health.

Discussion

Our study demonstrates that top-down control by soil fauna can restructure soil microbial communities to enhance pathogen suppression and ecosystem function. Rather than broadly stimulating microbial activity[12,13,22,24], nematode predation suppressed dominant bacterial taxa and promoted the proliferation of less abundant but functionally relevant species, leading to increased community evenness (Fig. 2). This community shift enhanced microbial traits essential for pathogen suppression, including broader carbon substrate utilization and a stronger functional signal related to antibiotic production

https://doi.org/10.1038/s41467-026-70413-3

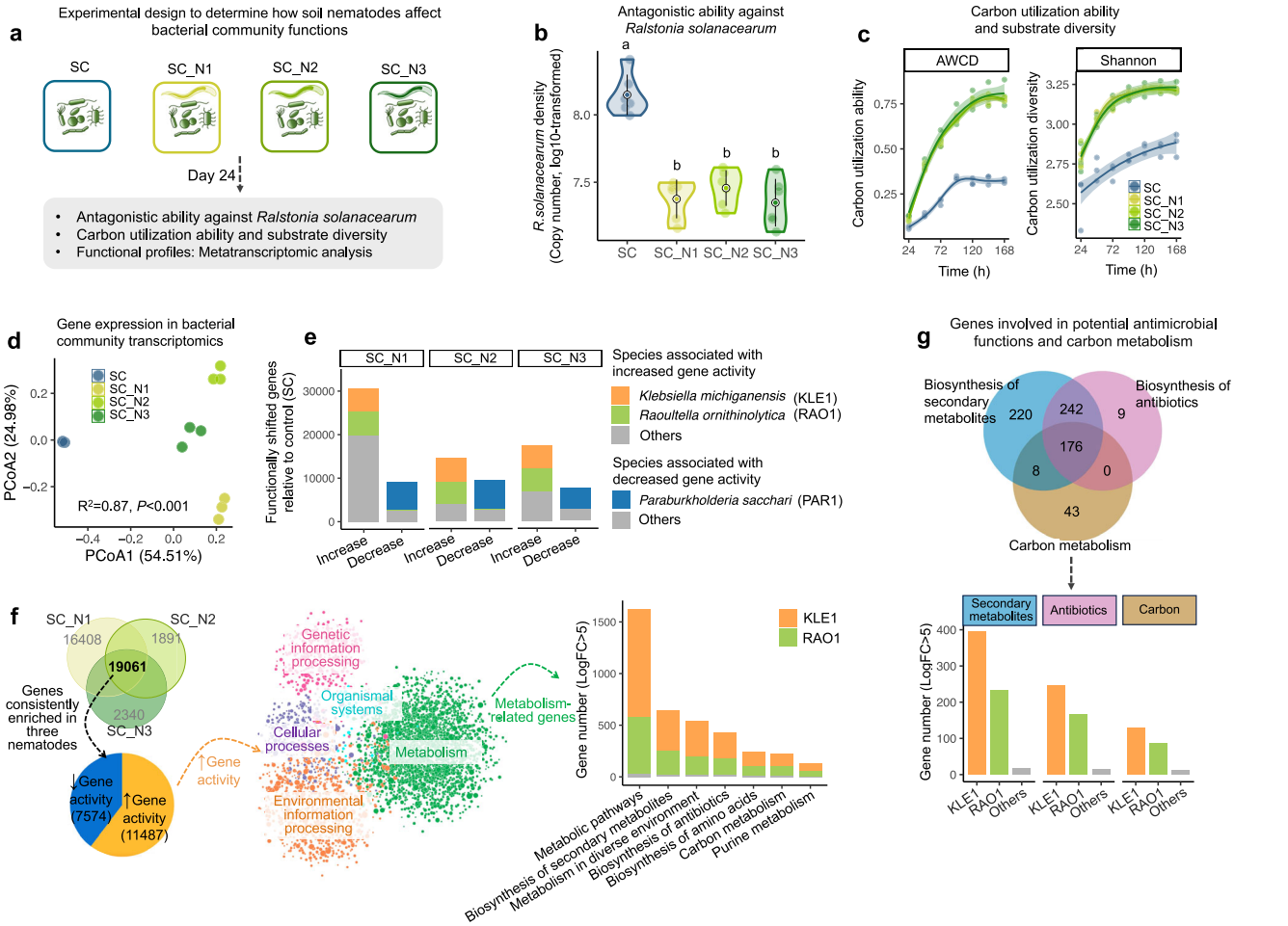

Fig. 3 | Nematode predation enhances bacterial functions in pathogen suppression and carbon utilization. a Experimental design to assess the impact of nematodes on bacterial community functions at the final sampling time (day 24), including measurements of antagonistic activity against *Ralstonia solanacearum*, carbon metabolism (via BioLog analysis), and metatranscriptome analysis. **b** The bacterial community suppresses *R. solanacearum* more effectively with nematodes ($n = 6$ biological replicates per treatment). Data are presented as mean ± SD, with individual data points showing the distribution. Different lowercase letters indicate significant differences among treatments ($P < 0.05$, Kruskal-Wallis chi-squared test with Dunn's post-hoc test). **c** The bacterial community utilizes carbon resources more effectively with nematodes ($P < 0.001$, Kruskal-Wallis chi-squared test; $n = 3$ biological replicates per treatment). The average well color development (AWCD) quantifies community metabolic activity, whereas the Shannon index indicates the diversity of carbon sources used by bacterial communities. Data are presented as LOESS fit with 95% confidence intervals (CI), with individual data points showing the distribution. **d** Aggregate gene abundance profiles of the bacterial community are altered by nematodes ($P < 0.001$, PERMANOVA by adonis; $n = 3$ biological replicates per treatment). **e** Nematodes influence bacterial functional profiles, increasing the activity of genes associated with KLE1 and RAO1, while decreasing those linked to PAR1 ($n = 3$ biological replicates per treatment). **f** Nematodes stimulate metabolic functions in the bacterial community, with KLE1 and RAO1 contributing prominently to enriched KEGG functional categories like secondary metabolite and antibiotic biosynthesis. The enriched genes and associated functions are clustered into distinct modules, with bubble size indicating LogFC values. The stacked bar plot shows the number of genes (LogFC > 5) involved in the top seven KEGG-defined metabolic pathways, along with their corresponding bacterial species. **g** KLE1 and RAO1 play dominant roles in the enrichment of genes (LogFC > 5) related to potential antimicrobial functions (biosynthesis of secondary metabolites and antibiotics) and carbon metabolism, based on KEGG pathway classifications. All results are based on metatranscriptomic differential analysis and reflect aggregate shifts in both bacterial population size and transcriptional activity.

(Fig. 3). These results support our hypothesis that nematode predation activates microbial traits contributing to pathogen suppression and enhance community-level functional capacity.

This functional enhancement arises from predator-facilitated interactions between functionally distinct microbial taxa. Nematodes selectively enriched Proteobacteria species such as *Klebsiella michiganensis* (KLE1) and *Raoultella ornithinolytica* (RAO1), both of which suppressed the pathogen *R. solanacearum*. These taxa exhibited metabolic complementarity: RAO1-conditioned medium stimulated KLE1 growth, while KLE1 supported superior nematode performance (Fig. 4). When these bacteria were combined with nematodes, their suppressive effects were amplified beyond pairwise interactions, suggesting that top-down pressure not only restructures microbiomes but also facilitates complex, beneficial interspecies interactions[25,26]. These findings support our second hypothesis and highlight the significance of trophic networks in shaping the emergent functions of the microbiome.

Two mechanisms likely underlie these effects. First, predators alter the species composition and interaction networks of lower trophic levels, primarily through selective feeding and biomass turnover[3,13,21]. These processes suppress taxa such as Firmicutes and Actinobacteria, which are often avoided by nematodes due to their thick cell walls or chemical defenses[17,19,20,27], while enriching fast-growing, predator-tolerant, and metabolically flexible Proteobacteria like KLE1 and RAO1. These shifts favor microbial traits conducive to coexistence and synergistic interactions, leading to communities better structured for functional complementarity[28,29]. Second, predation optimizes the microbiome's metabolic environment. The broader spectrum of carbon substrate utilization under nematode pressure

https://doi.org/10.1038/s41467-026-70413-3

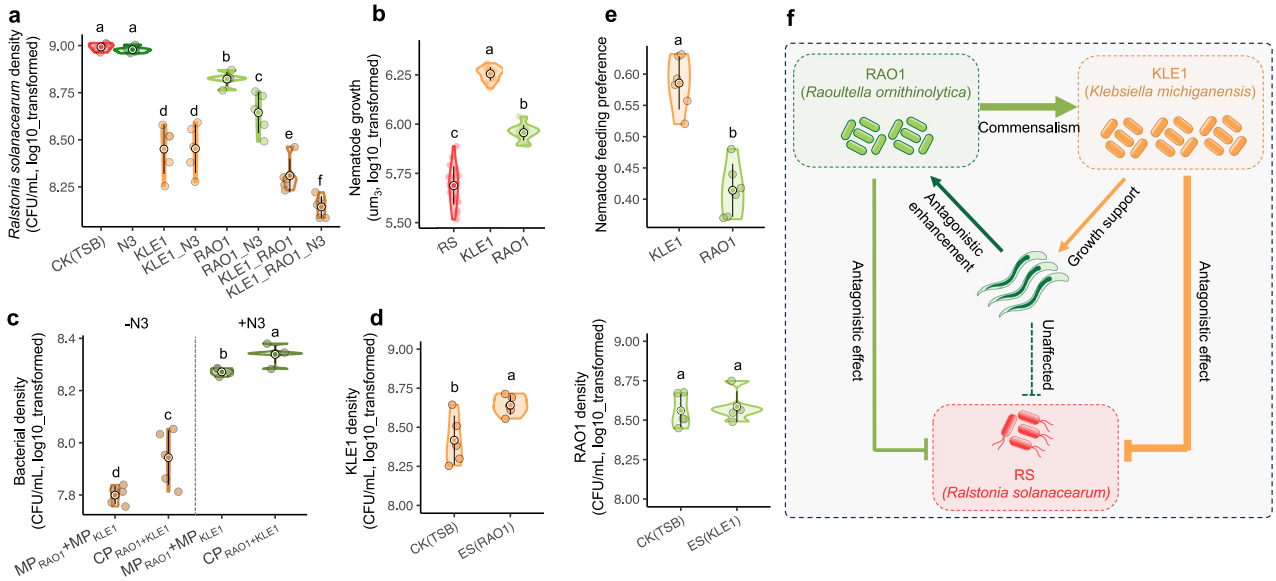

Fig. 4 | Trophic networks among nematodes and bacteria form a feedback loop that enhances pathogen resistance. a The tripartite interaction among KLE1, RAO1, and nematodes (N3, *Panagrolaimus* sp. NJ) leads to the most significant reduction in *Ralstonia solanacearum* density ($P < 0.05$, one-way ANOVA with LSD test; $n = 6$ biological replicates per treatment). **b** KLE1 promotes nematode growth (reflected by body size) more effectively than RAO1 and *R. solanacearum* (RS) ($P < 0.05$, one-way ANOVA with LSD test; $n = 20$ biological replicates per treatment). **c** Bacterial density is enhanced in the coculture of KLE1 and RAO1, particularly in the presence of nematodes ($P < 0.05$, one-way ANOVA with LSD test; $n = 6$ biological replicates per treatment). MP refers to monocultures of RAO1 and KLE1 grown separately; CP refers to their co-culture in the same medium. **d** RAO1 promotes KLE1 growth through extracellular secretions ($P < 0.05$, one-way ANOVA with LSD test; $n = 6$ biological replicates per treatment). The left panel shows the density of KLE1 cultured with extracellular secretions of RAO1, and the right panel shows the density of RAO1 cultured with extracellular secretions of KLE1. **e** Nematodes prefer KLE1 over RAO1 in a two-choice assay ($P < 0.05$, one-way ANOVA with LSD test; $n = 6$ biological replicates per treatment). For (**a**–**e**), data are presented as mean ± SD, with individual data points showing the distribution, and different lowercase letters indicating significant differences ($P < 0.05$). **f** Schematic illustration of nematode-mediated interactions with KLE1 and RAO1 shows high efficiency in suppressing *R. solanacearum*. Specifically, RAO1 and KLE1 share a commensal relationship, where KLE1 benefits from the presence of RAO1. Both RAO1 and KLE1 exhibit antagonistic effects against *R. solanacearum*. While nematodes cannot directly reduce *R. solanacearum* density through predation, their presence enhances the antagonistic effect against *R. solanacearum*.

(Fig. 3) indicates enhanced niche partitioning and metabolic differentiation. These features promote resource sharing among compatible taxa, which, in turn, buffers the community against environmental fluctuations and helps maintain pathogen-suppressive functions[30,31]. Together, these mechanisms suggest that predators act not only as consumers but also as ecological architects, enhancing microbiome resilience and functional performance.

Our findings challenge microbe-centric models of disease suppression[6–8,32,33] and advance a multitrophic framework in which faunal predators actively shape microbiome function and plant health through multispecies interactions[15]. The consistency of effects from these interactions across contexts spanning laboratory microcosms, experimental greenhouses, and agricultural fields supports the notion that nematodes are keystone species orchestrating bacterial interaction networks in soils to produce emergent beneficial outcomes for plant health and pathogen suppression. These insights open new avenues for microbiome engineering that explicitly incorporate faunal contributions and trophic complexity. Designing microbial consortia with trophic compatibility, such as prioritizing predator-favored taxa like Proteobacteria over commonly used Firmicutes that are poorly integrated into native trophic networks[34,35], may activate native food web interactions and enhance pathogen suppression with reduced chemical inputs. Future work should test the generality of these trophic mechanisms across soil types, cropping systems, and faunal communities to inform sustainable, multitrophic approaches to crop protection.

Methods

Farmland investigation sampling

The regional-scale farmland investigation was conducted in Jiangxi Province, southeastern China, spanning between 24°29′14″N-30°04′43″N and 113°34′18″E-118°28′56″E. This region experiences a subtropical warm and humid monsoon climate, characterized by an average annual temperature ranging from 16 °C to 25 °C and an annual precipitation of 1341 to 1943 mm. In summer 2022, we collected 124 tobacco rhizosphere soil samples across sites where tobacco is typically rotated with late rice and often planted on ridged paddy land. This rotation system has long been practiced in the region. Sampling locations were on the province's dominant red soils (FAO: Acrisols) and paddy soils, and tobacco bacterial wilt caused by the *Ralstonia solanacearum* species complex is widespread in this region. Each location was sampled with 8 to 10 plants to collect rhizosphere soils, which were then combined to create a single composite plot sample. The relative abundance of *R. solanacearum* was obtained through the analysis of 16S ribosomal DNA gene sequences using Illumina sequencing. Soil nematodes were extracted from 100 g of fresh rhizosphere soil using a combination of modified Baermann trays and centrifugal flotation methods[36].

Bacterial and nematode species

The synthetic bacterial community, consisting of 122 species, was isolated from the rhizosphere of tomato plants. Each bacterium was derived from a single clone and identified through 16S rDNA sequencing (Supplementary Table 1). Every bacterium was cultured using TSB medium (15 g L^{-1} Tryptone, 0.5 g L^{-1} Soytone, 0.5 g L^{-1} NaCl) at 30 °C.

The model nematode species *Caenorhabditis elegans* N2 was cultured in the laboratory as standard practice. The other three soil-dwelling nematode species (*Pristionchus quartusdecimus*, *Distolabrellus veechi* and *Panagrolaimus* sp.) were isolated from the rhizosphere of tomato plants and identified based on morphology and 18S rDNA (NCBI accession number: OQ832773, PX736993, PX736994).

https://doi.org/10.1038/s41467-026-70413-3

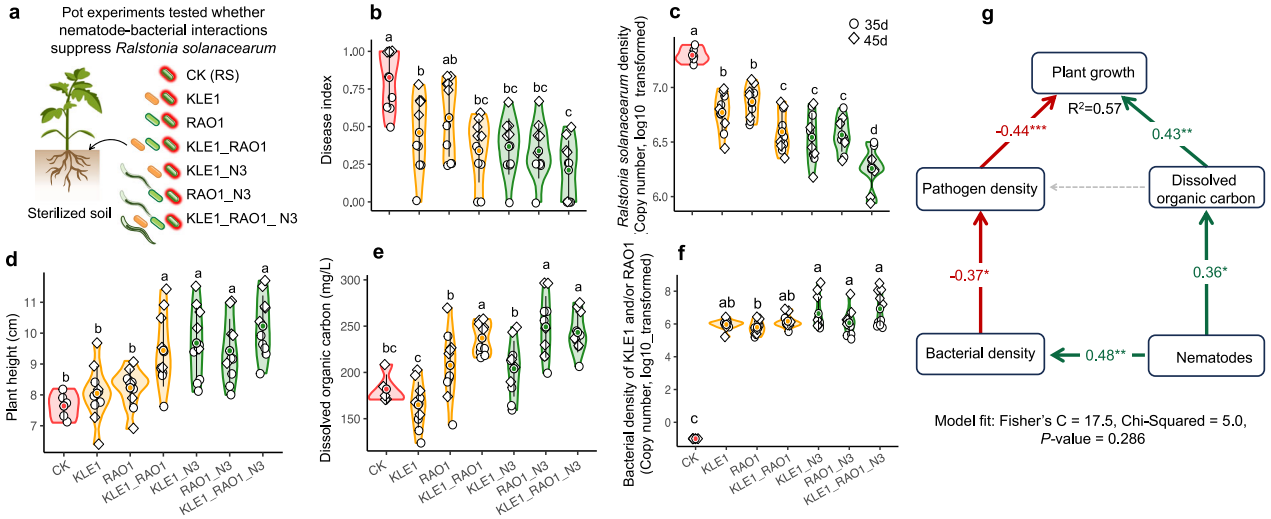

Fig. 5 | Rhizosphere nematode-bacterial interactions suppress pathogens and promote plant growth. a A greenhouse pot experiment using sterilized soil was conducted to test whether nematode-bacteria cooperation suppresses *R. solanacearum*, with $n = 10$ biologically independent plots/plants per treatment across two sampling times (day 35 and day 45). The control (CK) was inoculated with *R. solanacearum* alone, while other treatments were inoculated with *R. solanacearum* combined with KLE1, RAO1, or both, either with or without the nematode species (N3, *Panagrolaimus* sp. NJ). Sampling was conducted on days 35 and 45, when the control plants showed disease symptoms. **b**–**e** Nematodes coordinating with KLE1 and RAO1 reduce disease incidence (**b**; $P < 0.05$, Kruskal-Wallis chi-squared test with Dunn's post-hoc test) and *R. solanacearum* density (**c**; $P < 0.05$, one-way ANOVA with LSD test), promote tomato plant height (**d**; $P < 0.05$, one-way ANOVA with LSD test), and increase dissolved organic carbon concentrations (**e**; $P < 0.05$, one-way ANOVA with LSD test) ($n = 10$ biological replicates per treatment). **f** Nematode-bacteria interactions create positive feedback on bacterial density ($P < 0.05$, Kruskal-Wallis chi-squared test with Dunn's post-hoc test; $n = 10$ biological replicates per treatment). For (**b**–**f**), data are presented as mean ± SD, with individual data points showing the distribution, and different lowercase letters indicating significant differences ($P < 0.05$). **g** Piecewise structural equation model (SEM) shows how nematodes impact antagonistic bacteria, leading to carbon enrichment, pathogen suppression, and improved plant growth (day 45). Plant growth was quantified as a composite variable combining aboveground dry biomass and plant height using principal component analysis. The first principal component, explaining 73.8% of the variance, was extracted for model analysis. Arrows represent relationships: solid green and red arrows indicate positive and negative relationships, respectively, while dashed grey arrows represent non-significant relationships. A *P*-value (chi-square) > 0.05 indicates a good model fit.

We selected free-living nematodes that (i) were dominant in the field survey of rhizosphere communities, (ii) were easy to culture and manipulate, and (iii) exhibited similar developmental rates (L1 to egg-laying in 4–6 days), enabling synchronized and well-controlled microcosm and greenhouse assays. All nematodes were cultivated on NGM agar plates with *Escherichia coli* OP50 at 20 °C. The NGM medium consisted of 2.5 g L^{-1} Peptone, 3 g L^{-1} NaCl and 17 g L^{-1} agar. Before use, 25 mL 1 M KH_2PO4-K_2HPO_4 Buffer (pH 6.0), 1 mL 1 M $CaCl_2$, 1 mL 1 M $MgSO_4$ and 1 mL 5 mg/mL cholesterol were added sequentially to 1 L NGM medium. Tryptone, Soytone, Peptone, and chemical reagents were purchased from OXOID (UK) and Sangon Biotech (China). Soil-dwelling nematodes were synchronized at least five times to eliminate any potentially carried microbes from the natural environment.

Experimental setup and sampling

To explore the impact of nematode consumers on bacterial community coexistence and functions, we designed four treatments: control (synthetic bacterial community only), *C. elegans*, *D. veechi*, and *Panagrolaimus* sp. (each with synthetic bacterial community). Each treatment had six replicates and four sampling points, leading to a total of 96 microcosms (Fig. 2a). The microcosm experiment was conducted in 60 mm diameter culture plates using a fresh soil suspension to mimic the soil environment. Specifically, 60 g of fresh tomato-cultivated soil was combined with 120 mL PBS (pH 7.0) in a shaker for 4 h to create a soil suspension. After centrifugation at 5000 *g* for 5 min, a sterile soytone solution was added to the soil suspension, resulting in a final concentration of 0.05 % (W/V). This soil suspension mixture was then filtered twice through a 0.22 μm filter for future use.

Each bacterium was cultured overnight and adjusted to a density of 0.5 (OD600 nm). The 122 bacterial species were pooled in equal proportions (1:1…:1), washed three times in M9 buffer to remove residual culture medium, and inoculated into soil-suspension microcosms to create the synthetic bacterial community. A 1 mL volume of synthetic bacteria was added to 10 mL of soil suspension and adjusted to a density of 0.1 (OD600 nm), followed by transferring 10 mL of the resulting suspension into the culture plate. Approximately 200 synchronized nematode individuals at the L4 stage (the fourth larval stage immediately prior to adulthood) were added, with six biological replicates per treatment. Microcosms were maintained at 20 °C with gentle shaking for 6 days before transferring 5 mL to new culture dishes containing 5 mL of fresh soil suspension. This process continued for a total of 4 transfers over 24 days. Bacterial density, nematode numbers (excluding eggs), and 16S rDNA amplicon sequencing for bacterial community in both the soil suspension and nematode gut were measured before each transfer. Antagonistic ability against *R. solanacearum*, BioLog system analysis, and Metatranscriptome sequencing for bacterial functional profiles were conducted at the final sampling point.

DNA extraction

To extract microbial DNA from soil suspension, 2 mL of the culture suspension was transferred into an injector equipped with a 300-mesh filter membrane to remove nematodes. To isolate bacterial cells, the filtered culture suspension was centrifuged at 15,000 × *g* for 1 min. The resulting bacterial pellet was then used for total DNA extraction using the DNeasy 96 Blood & Tissue Kit (Qiagen, Germany), following the manufacturer's guidelines.

To extract microbial DNA from the nematode gut, 200 nematode individuals were selected and transferred to 1.5 mL tubes and washed with M9 buffer five times. Then, M9 buffer containing 10 mM levamisole was added to immobilize nematodes for 10 min, followed by the

addition of a 2-fold volume of disinfectant M9 buffer (1% NaClO and 0.25 M NaOH) to kill bacteria for 3 min. The mixture was then centrifuged at 600 *g* for 1 min to remove the supernatant, and the nematodes were washed with M9 buffer three times. The final wash buffer was spread onto a TSB plate to confirm successful sterilization. The remaining nematodes were lysed using an electric grinder (JingXin, China) equipped with a sterile broach to release bacteria into the solution. Total DNA was extracted using the DNeasy 96 Blood & Tissue Kit (Qiagen, Germany), following the manufacturer's guidelines.

16S rDNA amplicon sequencing and analysis

The V3-V4 region of the bacterial 16S rDNA gene was amplified using the primer pair 341 F (5′-barcode-CCT AYG GGR BGC ASC AG-3′) and 806 R (5′-GGA CTAC NNG GGT ATC TAA T-3′), where each sample had a unique eight-base barcode. Amplicons were then extracted from 2 % agarose gels and purified using the AxyPrep DNA Gel Extraction Kit (Axygen, USA), following the manufacturer's instructions. Purified PCR products were quantified using the Qubit® 3.0 (Life, USA), and twenty-four amplicons with distinct barcodes were equally combined. The pooled DNA product was used to construct Illumina Pair-End library following Illumina's genomic DNA library preparation procedure (https://support-docs.illumina.com/LP/IlluminaDNAPrep/Content/LP/Illumina_DNA/DNA-Prep/Protocol_IDP.htm). Subsequently, the amplicon library underwent paired-end sequenced (2 × 250) on an Illumina platform (BIOZERON Biotech., China) according to the standard protocols.

Raw fastq files were first demultiplexed using in-house perl scripts based on barcode sequence information for each sample. The following criteria were applied: (i) The 250 bp reads were truncated at any position with an average quality score <20 over a 10 bp sliding window. Truncated reads shorter than 50 bp were discarded. (ii) Exact barcode matching was employed, with a tolerance of up to two nucleotide mismatches allowed in primer matching. Reads containing ambiguous characters were removed. (iii) Sequences that overlapped by at least 10 bp were assembled based on their overlapping sequence. Unassembled reads were excluded. Operational taxonomic units (OTUs) were clustered at a 97% similarity cutoff using UPARSE (version 7.1 http://drive5.com/uparse/), and potential chimeric sequences were identified and removed using UCHIME. The phylogenetic affiliation of each 16S rDNA gene sequence was determined using the uclust algorithm (http://www.drive5.com/usearch/manual/uclust_algo.html), with a confidence threshold of 80%. The database of 16S rRNA gene fragments was constructed using the synthetic bacterial community composed of 122 species. All 16S rDNA gene sequences were compared to the established database using BLASTN, with a 97% similarity cutoff.

Nematode-mediated SynCom antagonism capacity: *R. solanacearum* suppression assay

To assess the impact of nematode predation on the SynCom's ability to suppress *R. solanacearum* QL-Rs1115, at the final sampling time (day 24) of the microcosm experiment, culture suspensions from each treatment were transferred into 50 mL tubes and centrifuged at 10,000 × *g* for 3 min to pellet the bacterial cells and nematodes. The supernatant was collected and filtered through a 0.22 μm filter to obtain cell-free filtrates, and mixed with NA medium (glucose 10 g L^{-1}, tryptone 5 g L^{-1}, beef extract 3 g L^{-1}, yeast extract 0.5 g L^{-1}) at ratio of 1:1 (V/V). *R. solanacearum* QL-Rs1115 was cultured overnight and inoculated into the mixed medium at 1 %. After incubation at 30 °C with shaking at 220 rpm for 24 h, the abundance of QL-Rs1115 was quantified by serial dilution and plate counting.

Nematode-mediated SynCom carbon utilization: BioLog analysis

BioLog EcoPlate, consisting 96 wells with 31 carbon sources, was used to assess the carbon metabolism of nematode-mediated SynCom. Briefly, 1 mL of the culture suspension was centrifuged at 15, 000 × *g* for 1 min, after which the supernatant was discarded. The pellet was washed with sterile water three times, and added to 9 mL of sterile 0.85 % NaCl (10^{-1}). A vortex mixer was used to ensure uniform mixing, and serial dilutions were made to achieve 10^{-3} concentration. A 150 μL aliquot of the dilution was added to the EcoPlates, which was then incubated at 25 °C. Absorbance readings were taken at 590 nm and 750 nm every 24 h up to 168 h. To correct for background absorbance, the readings for individual substrates were corrected by subtracting the absorbance of the control well (water) and the absorbance of the first reading. The average metabolic activity, indicated by average well color development (AWCD), was calculated using the formula: AWCD = Σ(C590-C750)/31, where C590 and C750 represent the optical density values at 590 nm and 750 nm from each well, respectively, with correlations for blank well values (inoculated with distilled water).

Nematode-mediated SynCom functional profile: Metatranscriptome sequencing and analysis

RNA extraction and library preparation. Total RNA was extracted from rhizosphere samples using TRIzol® Reagent (Invitrogen) following the manufacturer's instructions, and residual genomic DNA was removed using DNase I (TaKaRa). RNA quantity and integrity were assessed using a NanoDrop 2000 (Thermo Fisher Scientific) and an Agilent 2100 Bioanalyzer. Ribosomal RNA was depleted using the Ribo-Zero™ rRNA Removal Kit (Illumina), and cDNA libraries were constructed from 5 μg of total RNA using the TruSeq™ Stranded Total RNA Library Prep Kit (Illumina). Following fragmentation, cDNA synthesis, end repair, adaptor ligation, and PCR enrichment (15 cycles with Phusion DNA polymerase, NEB), target fragments of 200–300 bp were size-selected on a 2% Low Range Ultra Agarose gel. Libraries were sequenced on the Illumina NovaSeq 6000 platform (BIOZERON Biotech, China), generating paired-end reads (2 × 150 bp).

Data processing and functional annotation. Raw reads were quality-trimmed using Trimmomatic v0.36 (parameters: SLIDINGWINDOW:4:15 MINLEN:75). Reads aligning to the host genome were filtered out. Gene prediction was performed using MetaProdigal, and a non-redundant gene catalog was built using CD-HIT with 95% identity and 90% coverage. Functional annotations were assigned via BLASTp (v2.8.1 +) against the NCBI NR, KEGG, and STRING databases using an E-value cutoff of 1e-5. Gene Ontology (GO) terms were annotated using BLAST2GO.

Differential expression and pathway analysis. Transcript quantification was performed using Salmon (https://github.com/COMBINE-lab/salmon), and gene abundances were further normalized using RSEM. Differentially expressed genes (DEGs) between nematode-inoculated and control treatments were identified using edgeR (v3.36.0). Genes with an absolute $\log_2$ fold change > 2 and FDR < 0.05 were considered significantly changed in transcript signal. As transcript counts in metatranscriptomic data reflect both the abundance of gene templates (i.e., species-level DNA copy number) and mRNA transcriptional activity, all differential analyses were interpreted as aggregate transcript signal changes, representing the combined effects of population abundance shifts and transcriptional regulation. GO enrichment and KEGG pathway analysis were conducted using GOATOOLS and KOBAS, respectively. Enrichment was considered significant at Bonferroni-corrected $P < 0.05$.

Functional categorization and taxonomic assignment. To evaluate the impact of nematodes on bacterial functional profiles, we focused on genes with consistently increased aggregate transcript signal across all three nematode-inoculated treatments. Highly upregulated genes ($|\log_2 FC| > 5$) were extracted for downstream interpretation. DEGs were categorized into five major functional groups: metabolism,

environmental information processing, genetic information processing, cellular processes, and organismal systems. Among these, we focused on the seven most enriched KEGG pathways: metabolic pathways, biosynthesis of secondary metabolites, metabolism in diverse environments, biosynthesis of antibiotics, biosynthesis of amino acids, carbon metabolism, and purine metabolism. The number of genes with increased signal in each pathway was quantified and linked to species-level taxonomic annotations, based on the mapping of transcripts to the non-redundant gene catalog.

Nematode feeding preference between *Klebsiella michiganensis* (KLE1) and *Raoultella ornithinolytica* (RAO1)

Nematode feeding preference was assessed using bacteria's attractive index to nematodes. The attractive index was determined using the conventional method outlined in previous studies[37,38]. Briefly, a 90 mm culture plate was divided into sections with 200 adult nematodes placed at the center and two bacterial suspensions (each 20 µL) in marginal circles, including one of the bacteria and model bacterium *E. coli* OP50. Attraction was recorded at 8, 12, 24, and 36 h. The attraction index (AI) was calculated as Ni / (Ni + N_{OP50}), where Ni represents the number of nematodes in the dot-circle of bacteria i, and N_{OP50} represents the number of nematodes in the dot-circle of another bacterium *E. coli* OP50.

Interaction among the nematode, Klebsiella michiganensis (KLE1), Raoultella ornithinolytica (RAO1) and Ralstonia solanacearum (QL-Rs1115)

The antagonistic abilities of nematodes, KLE1, and RAO1 against QL-Rs1115 were evaluated using eight treatments: QL-Rs1115 alone, QL-Rs1115 + nematode, QL-Rs1115 + bacteria (KLE1, RAO1, or KLE1 + RAO1), and QL-Rs1115 + nematode + bacteria, with five replicates per treatment. Nematodes were synchronized and cultured to the L4 stage, washed with M9 buffer, and starved for 12 h. KLE1 and RAO1 were diluted to an OD_{600} of 0.6. A total of 1500 nematodes and 30 µL of bacterial suspension were added to 50 mL sterile tubes containing 3 mL NGM + 1% TSB medium and incubated at 22 °C with shaking at 120 rpm for 24 hours. After centrifugation, supernatants were filtered to obtain sterile extracellular secretions. QL-Rs1115 was cultured in NA medium, diluted to an OD_{600} of 0.4. 1.5 mL of QL-Rs1115 suspension was inoculated into an equal volume of either NGM + 1% TSB medium or the collected extracellular secretions. The mixtures were incubated at 30 °C and 180 rpm for 12 h Colony-forming units (CFUs) were counted.

Nematode body size was used as an integrative proxy for consumer performance and prey profitability on each bacterial prey, complementing the feeding-preference assay. Body size was calculated as volume from length and width measurement: body size = (length × width^2) / 1.7. Nematodes were cultured on NGM plates seeded with *E. coli* OP50, QL-Rs1115, KLE1, or RAO1 at 22 °C until adulthood, then heat-fixed and observed under a stereomicroscope. Body dimensions were measured using Motic Images Plus 3.0 software, with 20 replicates per treatment.

The interaction between KLE1 and RAO1 was tested using extracellular secretions. KLE1 and RAO1 suspensions were diluted to OD_{600} of 0.4, centrifuged, and filtered to obtain extracellular secretions. Each 1.5 mL suspension was incubated in an equal volume of either fresh TSB or the extracellular secretions of the other strain, and incubated at 30 °C with shaking at 180 rpm for 12 hours. Colony-forming units (CFUs) were counted. Interaction effects were interpreted as follows: if CK (TSB) > ES (strain), extracellular secretions inhibited the other strain's growth; if equal, no significant effect was observed; and if less, extracellular secretions promoted growth. Here, CK (TSB) refers to bacterial count in standard TSB medium, while ES (strain) refers to bacterial count in the extracellular secretions of the other strain.

The effect of nematodes on the interaction between KLE1 and RAO1 was studied with six treatments: monoculture (KLE1, RAO1, KLE1 + nematodes, RAO1 + nematodes) and co-culture (KLE1 + RAO1 and KLE1 + RAO1 + nematodes), each replicated five times. Nematodes were synchronized and cultured to the L4 stage, washed with M9 buffer, and starved for 12 hours. KLE1 and RAO1 suspensions were diluted to OD_{600} of 0.4. A total of 1500 nematodes and 300 µL of bacterial suspension were added to 50 mL sterile tubes containing 3 mL NGM + 1% TSB medium and incubated at 22 °C with shaking at 120 rpm for 12 hours. Colony-forming units (CFUs) were counted. Interaction effects were interpreted as follows: if $MP_{KLE1} + MP_{RAO1} > CP_{KLE1+RAO1}$, the strains were competitive; if equal, the interaction was neutral; and if less, the strains were facilitative. Here, MP and CP represent bacterial counts from monoculture and co-culture treatments, respectively.

Pot experiments

The farmland soil and substrate were pre-mixed at a 1:1 ratio, then sterilized by irradiation at a dose of 90 kGy (Xiyue Technology Co. Ltd., Nanjing), and packed into sterile plastic cups, with each cup containing 300 g of the mixed soil. Tomato seedlings were grown in sterile seedling-raising plate with sterile substrate, and transplanted into the sterile plastic cups once they reached the four-leaf stage. For nematode and SynCom experiment: after a 7-day stabilization period, nematodes and SynCom were introduced, followed by root inoculation with red fluorescent protein-labeled QL-Rs1115 (tagged with the pYC12-mCherry plasmid, construction details are provided in our previous study[39]) 7 days later. For KLE1, RAO1 and nematodes experiment: after a 7-day stabilization period, nematodes, KLE1 and green fluorescent protein-labeled RAO1 (tagged with the pYC12-eGFP plasmid, construction details are provided in our previous study[39]) were introduced, followed by root inoculation with red fluorescent protein labeled QL-Rs1115 7 days later. Each treatment group consisted of 20 individual repeats. The plants were cultivated in a greenhouse with temperatures ranging from 24 °C to 30 °C, with regular watering using sterile water and rearrangement every 5 days. The severity of bacterial wilt disease was recorded as a mean of disease index of each plant using a scale ranging from 0 to 4 (0, no signs of wilting; 1, 1–25% leaf area wilted; 2, 26–50% leaf area wilted; 3, 51–75% leaf area wilted; and 4, 76-100% leaf area wilted).

The rhizosphere soil samples and plant samples were collected at 10 days and 20 days after inoculation with QL-Rs1115, with 5 replicates each sample. Nematode extraction using a modified Baermann method. Plant height was measured as the vertical distance from the base of the stem (at the root collar) to the top of the plant under natural growth conditions. The red fluorescent visualization of tomato stems was conducted using a Confocal Laser Scanning Microscope (Leica TCS sp8, Germany). The abundance of QL-Rs1115, KLE1, and RAO1 was determined using real-time quantitative PCR with fluorescent primers. The primers used are as follow, Rs-forward: 5′- AGT TCA TGT ACG GCT CCA AGG CCT AC −3′, Rs-reverse: 5′- CGC GCA GCT TCA CCT TGT AGA TGA AC-3′; KLE1-forward: 5′- CAT GGC ACT GAA ATG GAA CGG CTT TG-3′, KLE1-reverse: 5′- TAT CTG GGC GTC AAG CAG TGT ATT CC −3′; RAO1-forward: 5′- TCA AGG ACG ACG GCA ACT ACA AGA C −3′, RAO1-reverse: 5′- CCT CGA TGT TGT GGC GGA TCT TGA A −3′. All primers were synthesized by Genscript Biotech Corporation.

Ammonium nitrogen content in soil was determined using the indophenol blue colorimetric method, with absorbance measured at 625 nm using a UV-Vis spectrophotometer (UV-8000, Shanghai Yuanxi). Available phosphorus content in soil was determined using the molybdenum-antimony colorimetric method following sodium bicarbonate extraction, with absorbance measured at 625 nm using a UV-Vis spectrophotometer. Dissolved organic carbon content in soil was determined by deionized water extraction and measured using a total organic carbon analyzer (TOC-LCPH, Shimadzu Corporation, Japan).

Statistical analysis

All statistical analyses and data visualization were conducted using R (version 4.1.2). To compare variable means across multiple treatments, we first evaluated the data distribution and selected appropriate statistical methods accordingly. Data normality was assessed using the Shapiro-Wilk test. For datasets meeting the normality assumption, one-way analysis of variance (ANOVA), followed by least significant difference (LSD) post hoc tests was used to assess differences among treatments. When the normality assumption was violated, non-parametric methods were applied: the Wilcoxon rank-sum test for pairwise comparisons and the Kruskal-Wallis test for multiple group comparisons.

To explore cross-trophic interactions between bacterial taxa and nematode taxa (bacterivores, fungivores, omnivore-predators, and herbivores) at the regional-scale, we constructed co-occurrence networks from field-survey data using the iNAP platform[40] (https://inap.denglab.org.cn) and visualized them with Gephi 9.2. Networks were built separately for healthy and diseased soils based on a unified ASV table integrating bacterial and nematode datasets. Only bacterial ASVs with relative abundance > 0.01% and occurrence frequency > 10% were included. Co-occurrence patterns were inferred using the SparCC method with correlation thresholds of $|r| > 0.3$ and $P < 0.05$. To focus on pathogen-relevant interactions, bacterial ASVs associated with *R. solanacearum* and with nematode groups were extracted for further analysis. In the resulting networks, nodes represent ASVs and edges denote significant correlations.

To evaluate the effects of nematodes on bacterial community structure and functional profiles, we conducted a series of diversity and multivariate analyses. Alpha diversity indices, including species richness and Pielou's evenness, were calculated using the *vegan* package[41]. The 'loess' smoothing method was applied to create a smooth curve that captures the underlying trends in alpha diversity. Differences in bacterial community composition among treatments were visualized using non-metric multidimensional scaling (NMDS) based on Bray-Curtis dissimilarity and statistically tested using permutational multivariate analysis of variance (PERMANOVA, adonis function in the *vegan* package, 999 permutations). In addition, bacterial species were categorized as dominant (>10% relative abundance), sub-dominant (1-10%), or rare (<1%) to assess compositional shifts. We also calculated fold changes in the relative abundance of each species using the formula (X-control)/control, where X represents the average abundance across all sampling times in the nematode-inoculated treatment. To assess functional shifts in the bacterial community, principal coordinates analysis (PCoA) was performed on Euclidean distances derived from normalized metatranscriptomic data. Statistical significance of treatment effects on both taxonomic and functional profiles was tested using PERMANOVA (adonis function).

To evaluate the direct and indirect effects of nematodes on plant health, we performed piecewise structural equation modeling (SEM) using the *piecewiseSEM* package[42]. Plant growth was quantified as a composite variable combining aboveground dry biomass and plant height, with the first principal component (explaining 73.8% of the variance) used as the growth index for modeling. The SEM framework included key variables such as nematode presence, bacterial and pathogen densities, dissolved organic carbon, and plant growth. Each path was fitted as a linear model, and model fit was evaluated using Fisher's C statistic and chi-square test. A non-significant chi-square test ($P > 0.05$) indicated acceptable model fit.

Reporting summary

Further information on research design is available in the Nature Portfolio Reporting Summary linked to this article.

Data availability

All raw Amplicon sequencing and Metatranscriptome sequencing data generated in this study have been deposited in the NCBI Sequence Read Archive (SRA) under accession numbers SRR36246718–SRR36247145 (https://www.ncbi.nlm.nih.gov/sra/?term= SRR36246718). Additional data generated in the study are available on figshare and can be accessed at https://doi.org/10.6084/m9.figshare.30630011[43].

Code availability

The R code used for data analysis is available on figshare and can be accessed at https://doi.org/10.6084/m9.figshare.30630011[43].

References

1. Soliveres, S. et al. Biodiversity at multiple trophic levels is needed for ecosystem multifunctionality. *Nature* **536**, 456 (2016).
2. Guo, S. et al. Trophic interactions between predatory protists and pathogen-suppressive bacteria impact plant health. *ISME J.* **16**, 1932–1943 (2022).
3. Jiang, Y. et al. Trophic interactions as determinants of the arbuscular mycorrhizal fungal community with cascading plant-promoting consequences. *Microbiome* **8**, 1–14 (2020).
4. Thakur, M. P. & Geisen, S. Trophic regulations of the soil microbiome. *Trends Microbiol.* **27**, 771–780 (2019).
5. Gralka, M., Szabo, R., Stocker, R. & Cordero, O. X. Trophic interactions and the drivers of microbial community assembly. *Curr. Biol.* **30**, R1176–R1188 (2020).
6. Mendes, R. et al. Deciphering the rhizosphere microbiome for disease-suppressive bacteria. *Science* **332**, 1097–1100 (2011).
7. Kwak, M. J. et al. Rhizosphere microbiome structure alters to enable wilt resistance in tomato. *Nat. Biotechnol.* **36**, 1100–1109 (2018).
8. Zhou, X. et al. Cross-kingdom synthetic microbiota supports tomato suppression of Fusarium wilt disease. *Nat. Commun.* **13**, 7890 (2022).
9. Xu, X. et al. Protorhabditis nematodes and pathogen-antagonistic bacteria interactively promote plant health. *Microbiome* **12**, 221 (2024).
10. Liu, T., Hu, F. & Li, H. Spatial ecology of soil nematodes: perspectives from global to micro scales. *Soil Biol. Biochem.* **137**, 107565 (2019).
11. van den Hoogen, J. et al. Soil nematode abundance and functional group composition at a global scale. *Nature* **572**, 194–198 (2019).
12. Jiang, Y. et al. Nematode grazing promotes bacterial community dynamics in soil at the aggregate level. *ISME J.* **11**, 2705–2717 (2017).
13. Jiang, Y. et al. Nematodes and their bacterial prey improve phosphorus acquisition by wheat. *N. Phytol.* **237**, 974–986 (2022).
14. Jiang, G. et al. Bacterial wilt in China: history, current status, and future perspectives. *Front. Plant Sci.* **8**, 1549 (2017).
15. Guo, S. et al. Predatory protists reduce bacteria wilt disease incidence in tomato plants. *Nat. Commun.* **15**, 829 (2024).
16. Jousset, A. Ecological and evolutive implications of bacterial defences against predators. *Environ. Microbiol.* **14**, 1830–1843 (2012).
17. Li, G. et al. Metabolites limiting predator growth wane with prey biodiversity. *Proc. Natl. Acad. Sci. USA* **121**, e2410210121 (2024).
18. Li, G., Liu, T., Whalen, J. K. & Wei, Z. Nematodes: an overlooked tiny engineer of plant health. *Trends Plant Sci.* **29**, 52–63 (2023).
19. Chuai, H. et al. *Pseudomonadota* bridge cross-trophic interactions to suppress plant pathogens. *ISME J.* https://doi.org/10.1093/ismejo/wrag011 (2026).
20. Liu, T. et al. Food familiarity does not change nematode feeding behavior. *Soil Biol. Biochem.* **125**, 136–143 (2018).
21. Trap, J., Bonkowski, M., Plassard, C., Villenave, C. & Blanchart, E. Ecological importance of soil bacterivores for ecosystem functions. *Plant Soil* **398**, 1–24 (2016).

22. Fu, S., Ferris, H., Brown, D. & Plant, R. Does the positive feedback effect of nematodes on the biomass and activity of their bacteria prey vary with nematode species and population size? *Soil Biol. Biochem.* **37**, 1979–1987 (2005).
23. Samuel, B. S., Rowedder, H., Braendle, C., Félix, M.-A. & Ruvkun, G. *Caenorhabditis elegans* responses to bacteria from its natural habitats. *Proc. Natl. Acad. Sci. USA* **113**, E3941–E3949 (2016).
24. Griffiths, B. Microbial-feeding nematodes and protozoa in soil: their effectson microbial activity and nitrogen mineralization in decomposition hotspots and the rhizosphere. *Plant Soil* **164**, 25–33 (1994).
25. Feeney, W. E. et al. Predation drives recurrent convergence of an interspecies mutualism. *Ecol. Lett.* **22**, 256–264 (2019).
26. Abrams, P. A. & Matsuda, H. Positive indirect effects between prey species that share predators. *Ecology* **77**, 610–616 (1996).
27. Genilloud, O. Actinomycetes: still a source of novel antibiotics. *Nat. Prod. Rep.* **34**, 1203–1232 (2017).
28. Huet, S. et al. Insights into the biotic factors driving the outcome of coalescence events between soil bacterial communities. *ISME Commun.* **5**, ycaf048 (2025).
29. Coyte, K. Z., Schluter, J. & Foster, K. R. The ecology of the microbiome: networks, competition, and stability. *Science* **350**, 663–666 (2015).
30. Culp, E. J. & Goodman, A. L. Cross-feeding in the gut microbiome: ecology and mechanisms. *Cell Host Microbe* **31**, 485–499 (2023).
31. Amarnath, K. et al. Stress-induced metabolic exchanges between complementary bacterial types underly a dynamic mechanism of inter-species stress resistance. *Nat. Commun.* **14**, 3165 (2023).
32. Schlatter, D., Kinkel, L., Thomashow, L., Weller, D. & Paulitz, T. Disease suppressive soils: new insights from the soil microbiome. *Phytopathology* **107**, 1284–1297 (2017).
33. Wei, Z. et al. Initial soil microbiome composition and functioning predetermine future plant health. *Sci. Adv.* **5**, eaaw0759 (2019).
34. Fira, D., Dimkić, I., Berić, T., Lozo, J. & Stanković, S. Biological control of plant pathogens by *Bacillus* species. *J. Biotechnol.* **285**, 44–55 (2018).
35. Muras, A., Romero, M., Mayer, C. & Otero, A. Biotechnological applications of *Bacillus licheniformis*. *Crit. Rev. Biotechnol.* **41**, 609–627 (2021).
36. Liu, M. et al. A sequential extraction procedure reveals that water management affects soil nematode communities in paddy fields. *Appl. Soil Ecol.* **40**, 250–259 (2008).
37. Zhang, Y., Lu, H. & Bargmann, C. I. Pathogenic bacteria induce aversive olfactory learning in *Caenorhabditis elegans*. *Nature* **438**, 179–184 (2005).
38. Liu, T. et al. Soil fauna actively change their diet to survive stress. *Soil Biol. Biochem.* **162**, 108435 (2021).
39. Wei, Z. et al. Trophic network architecture of root-associated bacterial communities determines pathogen invasion and plant health. *Nat. Commun.* **6**, 8413 (2015).
40. Feng, K. et al. iNAP: an integrated network analysis pipeline for microbiome studies. *iMeta* **1**, e13 (2022).
41. Oksanen, J. et al. Package 'vegan'. *Community ecology package, version 2*, (2019).
42. Lefcheck, J. S. piecewiseSEM: piecewise structural equation modelling in r for ecology, evolution, and systematics. *Methods Ecol. Evol.* **7**, 573–579 (2016).
43. Liu, T. et al. Predator-driven microbial feedback loops promote plant health. *Figshare* https://doi.org/10.6084/m9.figshare.30630011 (2026).

Acknowledgements

This work was funded by the National Natural Science Foundation of China (42577332 to G.L. and 32522068 to T.L.), National Natural Science Foundation of Jiangsu Province, China (BK20250195 to T.L.), China Postdoctoral Science Foundation (2024M761143 and 2025T180695 to G.L.), Postdoctoral Fellowship Program of CPSF (GZC20251618 to G.L.), Jiangsu Funding Program for Excellent Postdoctoral Talent (2025ZB654 to G.L.) and the Fundamental Research Funds for the Central Universities (KYQN2023048 to G.L.). A.J. was supported by the grant National Natural Science Foundation of China W2431030.

Author contributions

G.L., L.T., H.L., and W.Z. conceived the project and designed research. G.L., H.C., H.M., and Z.Y. performed research. G.L., T.L., H.C., and S.H. conducted the statistical analysis. G.L., T.L., A.J., and S.H. wrote the first draft, the manuscript was subsequently revised and finalized based on the feedback from Y. X., Q.S., F.H., and S.G. All authors discussed and commented on the results and on the manuscript.

Competing interests

The authors declare no competing interests.

Additional information

Supplementary information The online version contains supplementary material available at https://doi.org/10.1038/s41467-026-70413-3.

Correspondence and requests for materials should be addressed to Ting Liu or Zhong Wei.

Peer review information *Nature Communications* thanks Holger Heuer, and the other, anonymous, reviewer(s) for their contribution to the peer review of this work. A peer review file is available.